

# 1 Quantifying POLNet Ozone Lidar Accuracy during the 2014 2 DISCOVER-AQ and FRAPPÉ Campaigns

3  
4 Lihua Wang<sup>1</sup>, Michael J. Newchurch<sup>1</sup>, Raul J. Alvarez II<sup>2</sup>, Timothy A. Berkoff<sup>3</sup>, Steven S. Brown<sup>2</sup>,  
5 William Carrion<sup>3,4</sup>, Russell J. De Young<sup>3</sup>, Bryan J. Johnson<sup>2</sup>, Rene Ganoë<sup>4</sup>, Guillaume Gronoff<sup>3,4</sup>,  
6 Guillaume Kirgis<sup>2,5</sup>, Shi Kuang<sup>1</sup>, Andrew O. Langford<sup>2</sup>, Thierry Leblanc<sup>6</sup>, Erin E. McDuffie<sup>2,5</sup>,  
7 Thomas J. McGee<sup>7</sup>, Denis Pliutau<sup>4</sup>, Christoph J. Senff<sup>2,5</sup>, John T. Sullivan<sup>7</sup>, Grant Sumnicht<sup>4</sup>,  
8 Laurence W. Twigg<sup>4</sup>, Andrew J. Weinheimer<sup>8</sup>

9

10 <sup>1</sup>University of Alabama in Huntsville, Huntsville, Alabama, USA

11 <sup>2</sup>NOAA Earth System Research Laboratory, Boulder, Colorado, USA

12 <sup>3</sup>NASA Langley Research Center, Hampton, Virginia, USA

13 <sup>4</sup>Science Systems and Applications Inc., Lanham, Maryland, USA

14 <sup>5</sup>Cooperative Institute for Research in Environmental Sciences, University of Colorado, Boulder, Colorado, USA

15 <sup>6</sup>Jet Propulsion Laboratory, California Institute of Technology, Wrightwood, California, USA

16 <sup>7</sup>NASA Goddard Space Flight Center, Greenbelt, Maryland, USA

17 <sup>8</sup>NOAA National Center for Atmospheric Research, Boulder, USA

18

19 Correspondence to Shi Kuang (kuang@nsstc.uah.edu)

20

## 21 Abstract

22 The Tropospheric Ozone Lidar Network (TOLNet) is a unique network of lidar systems that measure high-  
23 resolution atmospheric profiles of ozone. The accurate characterization of these lidars is necessary to determine the  
24 uniformity of cross-instrument calibration. From July to August 2014, three lidars, the TROPospheric OZone  
25 (TROPOZ) lidar, the Tunable Optical Profiler for Aerosol and oZone (TOPAZ) lidar, and the Langley Mobile Ozone  
26 Lidar (LMOL), of TOLNet participated in the “Deriving Information on Surface conditions from Column and  
27 Vertically Resolved Observations Relevant to Air Quality” (DISCOVER-AQ) mission and the “Front Range Air  
28 Pollution and Photochemistry Experiment” (FRAPPÉ) to measure ozone variations from the boundary layer to the top  
29 of the troposphere. This study presents the analysis of the intercomparison between the TROPOZ, TOPAZ, and LMOL  
30 lidars, along with comparisons between the lidars and other *in situ* ozone instruments including ozonesondes and a P-  
31 3B airborne chemiluminescence sensor. In terms of the range-resolving capability, the TOLNet lidars measured  
32 vertical ozone structures with an accuracy generally better than  $\pm 15\%$  within the troposphere. Larger differences occur  
33 at some individual altitudes in both the near-field and far-field range of the lidar systems, largely as expected. In terms  
34 of column average, the TOLNet lidars measured ozone with an accuracy better than  $\pm 5\%$  for both the intercomparison  
35 between the lidars and between the lidars and other instruments. These results indicate very good measurement  
36 accuracy for these three TOLNet lidars, making them suitable for use in air quality, satellite validation, and ozone  
37 modeling efforts.

## 38 1. Introduction

### 39 1.1 TOLNet

40 The Tropospheric Ozone Lidar Network (TOLNet) provides time-height measurements of ozone from the  
41 planetary boundary layer (PBL) to the top of the troposphere at multiple locations for satellite validation, model  
42 evaluation, and scientific research (Newchurch et al., 2016; <http://www-air.larc.nasa.gov/missions/TOLNet/>).  
43 Particularly, these high-fidelity ozone measurements can serve to validate NASA’s first Earth Venture Instrument  
44 mission, Tropospheric Emissions: Monitoring Pollution (TEMPO), planned to launch in 2019. A second objective of  
45 TOLNet is to identify a brassboard ozone lidar instrument that would be suitable to populate a network to address an  
46 increasing desire for ozone profiles by air-quality scientists and managers within the modeling and satellite  
47 communities (Bowman, 2013).

48 TOLNet consists of five ozone lidars across the United States and one in Canada: the Table Mountain  
49 tropospheric ozone differential absorption lidar (DIAL) at NASA’s Jet Propulsion Laboratory, the Tunable Optical  
50 Profiler for Aerosol and oZone (TOPAZ) lidar at NOAA’s Earth System Research Laboratory (ESRL), the Rocket-  
51 city Ozone ( $O_3$ ) Quality Evaluation in the Troposphere ( $RO_3QET$ ) lidar at the University of Alabama in Huntsville  
52 (UAH), the TROPospheric OZone (TROPOZ) DIAL at NASA’s Goddard Space Flight Space Center (GSFC), the  
53 Langley Mobile Ozone Lidar (LMOL) at NASA’s Langley Research Center (LaRC), and Autonomous Mobile Ozone  
54 Lidar Instrument for Tropospheric Experiments (AMOLITE) at Environment and Climate Change Canada.

55 All TOLNet lidars have unique configurations that are associated with their original measurement design  
56 purposes, including their transmitter, receiver, and signal processing systems. Most components of these lidars are  
57 customized and differ significantly in pulse energy, repetition rate, receiver size, solar (or narrow-band) interference  
58 filter, and range resolution. These differences result in varying signal-to-noise ratios (SNRs), which impact the useful  
59 operating ranges and statistical uncertainties in ozone retrieval. The selection of the DIAL wavelengths determines  
60 the sensitivity to interference by other species, primarily aerosols. In addition, multiple lidar data processing and  
61 retrieval algorithms could also lead to different effective resolutions and lidar retrieval uncertainties (Godin et al.,  
62 1999; Leblanc et al., 2016). Therefore, it is important to quantify the measurement differences between the TOLNet  
63 lidars and understand their sources before we form a consistent TOLNet dataset. A previous intercomparison between  
64 TROPOZ and LMOL reported by Sullivan et al. (2015) concluded that the observed ozone column averages from the  
65 two lidars were within  $\pm 8\%$  of each other, and their ozone profiles were mostly within  $\pm 10\%$  of each other. That  
66 particular study served as the first reported measurement intercomparison of two ground-based tropospheric ozone  
67 lidar systems within the United States.

## 68 **1.2 DISCOVER-AQ 2014 and FRAPPÉ Campaigns**

69 The scientific goal of the TOLNet lidars in this study was to provide continuous, high-resolution tropospheric  
70 ozone profiles to support the NASA-sponsored DISCOVER-AQ mission ([https://www.nasa.gov/larc/2014-](https://www.nasa.gov/larc/2014-discoveraq-campaign/)  
71 [discoveraq-campaign/](https://www.nasa.gov/larc/2014-discoveraq-campaign/)), and the National Science Foundation (NSF) and state of Colorado (CO) jointly sponsored  
72 FRAPPÉ (Dingle et al., 2016) from July to August 2014. By collaborating with FRAPPÉ, the 2014 CO study was the  
73 final stop in a series of four field campaigns by DISCOVER-AQ to understand sources, transport and chemical  
74 transformations of air pollutants, particularly those that lead to ground-level ozone formation (Crawford and Pickering,  
75 2014).

76 Prior to the two campaigns, TOPAZ, TROPOZ, and LMOL were all deployed to the same location in Erie,  
77 CO to obtain intercomparison data at the Boulder Atmospheric Observatory (BAO) (40.050°N, 105.003°W, 1584 m  
78 above sea level, ASL). Subsequent to the BAO intercomparison, TROPOZ and LMOL re-deployed to locations near  
79 Fort Collins, CO (~60 km north-northwest of BAO) and Golden, CO (~40 km southwest of BAO), respectively, for  
80 their different scientific missions. During the DISCOVER-AQ and FRAPPÉ campaigns, balloon-borne ozonesondes  
81 were launched at selective sites. In addition, the NASA P-3B aircraft performed multiple spiral ascents and descents  
82 over several ground sites and provided numerous vertical profiles of ozone measurements. In this study, we compare  
83 retrievals between the three lidars and evaluate the ozone lidar accuracy using ozonesonde and P-3B aircraft  
84 measurements. These two campaigns offered a unique opportunity for the lidar validation work, as they involved so  
85 many different instruments.

## 86 **2. Instruments**

### 87 **2.1 TOLNet Lidars**

88 **Table 1** lists the main hardware specifications of the three TOLNet lidars and their ozone retrieval processes,  
89 which could potentially impact the intercomparison result.

### 90 **2.1.1 TROPOZ/NASA GSFC**

91 The transmitter for TROPOZ consists of two 50-Hz Nd:YAG- lasers used to pump two Raman cells filled  
92 with Deuterium (D<sub>2</sub>) and Hydrogen (H<sub>2</sub>) gases, respectively, to generate two outgoing lasers at 289 and 299 nm. The  
93 typical pulse energies are 12 mJ at 299 nm (off-line) and 16 mJ at 289 nm (on-line) (Sullivan et al., 2014). The  
94 receiving system consists of a 45-cm-diameter Newtonian telescope for measuring far field and four smaller 2.5-cm  
95 refracting telescopes to measure near field. The 45-cm telescope has a 1-mrad field of view (FOV), and the 2.5-cm  
96 telescopes have a much wider FOV at 10 mrad. In each channel, solar interference filters with a 1-nm bandwidth  
97 decrease the amount of ambient solar light, which improves the SNR. The fundamental range resolution for the data  
98 acquisition system is 15 m (100 ns). TROPOZ measures ozone up to 16 km during daytime hours and higher altitudes  
99 at night.

### 100 **2.1.2 TOPAZ/NOAA ESRL**

101 The TOPAZ lidar is a truck-mounted zenith-looking, scanning instrument modified from the nadir-looking  
102 airborne DIAL configuration first used in the 2006 Texas Air Quality Study (TexAQ5 II) (Alvarez et al., 2011; Senff  
103 et al., 2010). The lidar transmitter is based on a Ce:LiCAF laser pumped by a quadrupled Nd:YLF laser to produce  
104 three UV wavelengths, each at a 333 Hz repetition rate and tunable from 283 nm to 310 nm. The actual wavelengths  
105 used during DISCOVER-AQ 2014 were 287, 291, and 294 nm. Compared to the conventional two-wavelength DIAL,  
106 the three-wavelength configuration can potentially minimize the aerosol interference by using the dual-DIAL retrieval  
107 technique (Kovalev and Bristow, 1996) without assuming a lidar ratio and Angström exponent. However, in this study,  
108 ozone was retrieved using the 287- and 294-nm lidar signals and the standard two-wavelength DIAL algorithm  
109 because the two-wavelength retrieval was less affected by significant lidar signal noise (Alvarez et al., 2011).

110 Laser light backscattered by air molecules and aerosol particles is collected with a co-axial 50-cm diameter  
111 Newtonian telescope and then split at a 1:9 ratio into near- and far-field detection channels. The FOVs of the near-  
112 and far-field channels are controlled by different-size apertures resulting in full overlap at distances of ~300 m and  
113 ~800 m, respectively. Both channels use gated photomultipliers (PMTs) operated in analog mode with solar  
114 interference filters during the daytime. Compared to photon counting (PC) signals, the analog signal is able to keep  
115 high linearity for strong signals and is particularly suitable for near-range measurement. The two-axis scanner on the  
116 truck permits pointing the laser beam at several shallow elevation angles at a fixed, but changeable azimuth angle,  
117 typically at 2°, 6°, 20°, and 90° elevation angles that are repeated approximately every 5 minutes. The ozone profiles  
118 at these four angles are spliced together to create composite vertical profiles extending from 10 m to about 2 km AGL  
119 (Langford et al., 2016). The range resolution of the signal recording system is 6 m.

120 During the 2014 DISCOVER-AQ and FRAPPÉ campaigns, the TOPAZ ozone observations at low elevation  
121 angles (2°, 6°, and 20°) suffered from a slight, but consistent range-dependent bias created by an unknown source of  
122 noise in the data acquisition system. The cause of this noise remains unknown and attempts to correct the resulting

123 bias were unsuccessful. This bias manifests itself primarily in the low-angle observations because the signal levels  
124 and SNR are significantly lower compared to the measurements at 90°. For these reasons, the low angle observations  
125 below 500 m were excluded from the comparisons reported within this study.

### 126 **2.1.3 LMOL/NASA LaRC**

127 The transmitter of LMOL consists of a diode-pumped Nd:YLF laser pumping a Ce:LiCAF tunable UV laser  
128 to obtain two wavelengths typically at 287.1 and 292.7 nm with a pulse energy of 0.2 mJ at 500 Hz for each  
129 wavelength. The lidar receiver system consists of a 40-cm telescope with a 1.4-mrad FOV to measure far field and  
130 another 30-cm telescope with an adjustable FOV to measure near field (De Young et al., 2017). The raw lidar signals  
131 are recorded with a 7.5-m range resolution. The LMOL data acquisition system operates in both analog and PC modes.  
132 In this study, LMOL measures ozone between 0.7 and 4.5 km. Ozone measurements for DISCOVER-AQ represent  
133 LMOL's very first remote deployment.

### 134 **2.1.4 Lidar Data Processing and Retrieval Algorithms**

135 The data processing and DIAL retrieval algorithms for the three TOLNet lidars are similar but not identical.  
136 Their details have been described by Alvarez et al. (2011), De Young et al. (2017), Langford et al. (2011), and Sullivan  
137 et al. (2015; 2014). Some basic procedures were applied on the raw lidar signals before retrievals, such as time  
138 integration (5 min for this study), dead-time correction (for PC only), background correction, merging of PC and  
139 analog signals (for a system with both PC and analog channels), and signal-induced-bias (SIB) correction (Kuang et  
140 al., 2013). Some parameters are system dependent or empirical due to different equipment, such as the dead-time  
141 value, PC-analog timing offset, averaging range for background calculation, and SIB simulation function. All groups  
142 agreed to use the Brion-Daumont-Malicet (BDM) database (Daumont et al., 1992; Malicet et al., 1995; Brion et al.,  
143 1993) to calculate differential ozone absorption cross-sections, which are temperature-dependent.

144 The ozone number density profile results from computing the derivative of the logarithm of the on-line to  
145 off-line signal ratios. Spatial smoothing is usually necessary to improve the SNR and reduce the statistical errors.  
146 Various smoothing methods and their impacts on final lidar retrieval have been described by Godin et al. (1999). Both  
147 TROPOZ and LMOL groups applied a Savitzky-Golay (SG) filter with a 2<sup>nd</sup> degree polynomial on the derivative of  
148 the logarithm of the on-line to off-line signal ratios with an increasing window width to accommodate the quickly  
149 decreasing SNR. However, the SG window sizes for TROPOZ and LMOL are different due to different SNRs at each  
150 altitude. The TOPAZ group smoothed the derivative with a five-point least-square fitting in a 450-m interval. The  
151 different retrieval methodologies and parameters affect the effective vertical resolution of the retrieved ozone profiles,  
152 as listed in Table 1. This effective resolution determines the capability of the lidars to resolve vertical ozone structure  
153 and is not equal to, but is associated with, the fitting window width.

154 All groups applied similar schemes to correct the aerosol interference. These schemes iteratively substitute  
155 derived ozone from the DIAL equation into the lidar equation to solve aerosol extinction and backscatter until both  
156 aerosol and ozone converge (Alvarez et al., 2011; Kuang et al., 2011; Sullivan et al., 2014). The differential aerosol  
157 backscatter and extinction were calculated with the approximation from Browell et al. (1985). Lidars directly measure

158 the ozone number density, and all three groups used the same temperature and pressure profiles from co-located  
159 ozonesonde measurements for Rayleigh correction, ozone mixing-ratio calculations, and computation of the  
160 temperature dependent ozone absorption cross sections.

161 Merging between different altitude channels, either different telescopes or different optical channels of the  
162 same telescope, is challenging with limited methodologies reported in the literature (Kuang et al., 2011). It is difficult  
163 to specify a method for all groups because merging is system-dependent and is affected by many factors previously  
164 described. Therefore, the three lidar groups merge the ozone profiles at different altitudes optimized for their system  
165 and SNR levels such as the example method described by Sullivan et al. (2015). As a result, additional differences  
166 between systems can occur due to the non-standardized altitude channel merging.

### 167 **2.1.5 Error budget of the lidar measurements**

168 Only a brief description of the error budget of the lidar measurements is provided in this paper since the  
169 details have been discussed by their own instrumentation literatures (Alvarez et al., 2011; De Young et al., 2017;  
170 Sullivan et al., 2014). Table 2 presents the estimated measurement uncertainties for 5 or 30-min integration time for  
171 the three lidars. Statistical errors (Papayannis et al., 1990) arising from signal and background noise fluctuations are  
172 random errors and may be improved by additional averaging or smoothing. The maximum statistical uncertainties for  
173 the three lidars are similar (20% for 5 min and 8% for 30 min) within their measurable ranges although they are  
174 different at the same altitude. The uncertainty arising from aerosol interference could be the largest systematic error  
175 source and can be minimized by using the appropriate correction algorithm (Eisele and Trickl, 2005; Immler, 2003;  
176 Sullivan et al., 2014). The estimated total lidar measurement uncertainties are 22% and 13% for 5 and 30 min,  
177 respectively, within the lidar measurement ranges listed in Table 1.

### 178 **2.2 Ozonesondes**

179 An ozonesonde is a lightweight, balloon-borne instrument that consists of a Teflon air pump and an ozone  
180 sensor interfaced to a meteorological radiosonde. The ozone sensor uses an electrode electrochemical cell containing  
181 potassium iodide (KI) solution (Komhyr, 1969; Komhyr et al., 1995) to measure ozone with a precision better than  
182  $\pm 5\%$  and an accuracy better than  $\pm 10\%$  up to 35 km altitude with a sampling interval of about 1 s and a retrieval  
183 vertical resolution of 100 m (Deshler et al., 2008; Johnson et al., 2008; Smit et al., 2007). As the balloon carrying the  
184 instrument package ascends through the atmosphere, the pump bubbles ambient air into the sensor cell. The reaction  
185 of ozone and iodide generates an electrical signal proportional to the amount of ozone. A radiosonde attached in the  
186 same package measures air temperature, pressure, and relative humidity (Stauffer et al., 2014). Ozonesondes are  
187 capable of measuring ozone under various weather conditions (e.g., cloudy, thunderstorm). The free-flying  
188 ozonesondes typically reach 35-km altitude in less than two hours with a rise rate at about 5 m/s.

### 189 **2.3 Ozone Measurement Instrument onboard NASA's P-3B**

190 NASA's P-3B aircraft is a pressurized, four-engine turboprop, capable of long-duration flights of 8-12 hours  
191 and is based out of NASA's Wallops Flight Facility in Wallops Island, Virginia. A series of gas and aerosol instruments  
192 were outfitted within the P-3B aircraft. Ozone was measured using the National Center for Atmospheric Research

193 (NCAR)'s 4-channel chemiluminescence instrument based on the reaction between ambient ozone and nitric oxide  
194 (NO) with an accuracy of about  $\pm 5\%$  and sampling interval of 1 s (Weinheimer et al., 1993; Ridley et al., 1992). The  
195 precision of this ozone detector is better than  $\pm 1\%$  when ambient ozone is higher than 10 ppbv. The P-3B aircraft flew  
196 spirals from 300 m to 4570 m above the surface over selected ground monitoring sites including all three lidar sites  
197 (more information in Section 3.3) during the DISCOVER-AQ 2014 campaign.

### 198 **3. Results**

#### 199 **3.1 Lidar Intercomparisons**

200 The three TOLNet lidars were deployed next to the BAO tower to take simultaneous measurements before  
201 the DISCOVER-AQ/FRAPPE campaign. They were only a few hundreds of meters away from each other and were  
202 within 5 m of the same elevation (see measurement locations in Table 1).

203 Unlike stratospheric ozone lidars that focus on integrating hours of observations, tropospheric ozone lidars  
204 need to detect ozone variations with timescales on the order of minutes, when considering ozone's shorter lifetime,  
205 smaller-scale transport, and mixing processes within the PBL and free troposphere (Steinbrecht et al., 2009;  
206 McDermid et al., 1990). Therefore, we processed all lidar data on a 5-min temporal scale (signal integration time).  
207 Rayleigh correction was performed with the same atmospheric profile from the ozonesonde. Because the three lidars  
208 have different fundamental range resolutions, retrieved ozone number density values were internally interpolated on  
209 the same altitude grid with a 15-m interval for comparison.

210 Figure 1 presents the comparison of the TOPAZ and TROPOZ observed ozone at BAO from 1300 to 2135  
211 UTC (6 hours ahead of local time, Mountain Daylight Time) on July 11, 2014 under a partly cloudy sky condition.  
212 Data influenced by cloud interferences were filtered out. Ozone curtains from both lidars (Figure 1 a and b) show a  
213 significant (about 40%) ozone increase in the early afternoon. A total of 7655 TOPAZ and TROPOZ coincident pairs  
214 were constructed between 0.6 and 2 km AGL (altitude range over which both lidars provided valid data) over this time  
215 period. The measurement differences between the two lidars are mostly within  $\pm 5\%$  at individual grids (Figure 1 c).  
216 The product of averaged ozone concentration over some specified altitude range can represent the atmospheric ozone  
217 abundance and can be also useful for satellite validation. Here, we refer this product as ozone column average with  
218 the unit of number density, not to be confused with integrated column ozone often with a unit of the Dobson Unit. The  
219 statistics of the intercomparison of the column averages is listed in Table 3. The similar  $1\sigma$  standard deviations ( $17.8$   
220 and  $16.7 \times 10^{16} \text{ molec}\cdot\text{m}^{-3}$ ) suggest similar ozone variations captured by both lidars. The mean relative difference (or  
221 normalized bias) was calculated by averaging the relative difference (i.e.,  $(\text{TROPOZ}-\text{TOPAZ})/\text{TOPAZ}$ , the  
222 denominator was arbitrarily chosen) for all paired ozone profiles. The  $-1.1\pm 2.6\%$  mean relative difference suggests  
223 excellent agreement of the averaged ozone column (Figure 1 d) for 80 profiles over 6.5 hours between TOPAZ and  
224 TROPOZ retrievals.

225 Figure 2 shows the TOPAZ-LMOL intercomparison for data taken on July 16, 2014 with 1902 coincident  
226 pairs from 0.9 to 2 km and between 1340 to 1730 UTC on this day. Some of the data gaps were due to low clouds  
227 blocking the lidar beams. The retrievals between the two lidars agree with each other mostly within  $\pm 10\%$  (Figure 2

228 c). LMOL measured ozone column average (Figure 2 d)  $3.8 \pm 2.9\%$  lower than TOPAZ on average with totally 28  
229 paired profiles, which is significantly fewer than those from the TROPOZ-TOPAZ comparison.

230 The generally random distribution of the relative differences in Figure 1 (c) and 2 (c) suggests overall  
231 consistent measurements with small systematic errors from all three lidars. In summary, TROPOZ, LMOL, and  
232 TOPAZ report ozone values at individual altitudes mostly within  $\pm 10\%$ , which is well within their respective  
233 uncertainties and report ozone column averages within  $\pm 3.8\%$  on average.

### 234 3.2 Lidars versus Ozonesondes

235 In order to compare the lidar data to ozonesondes, the Rayleigh- and aerosol-corrected lidar data was  
236 converted from ozone number densities to ozone mixing ratios by using sonde-measured pressure and temperature  
237 profiles, and averaged over a 30-minute interval ( $\pm 15$  minutes around sonde launch times). The ozonesondes report  
238 values approximately every second (about every 5 m in altitude) in raw data. For comparison, the ozonesonde raw  
239 data were linearly interpolated on the lidar altitude grids with a 15-meter interval. Figure 3 shows the mean ozone  
240 mixing ratios measure by TOLNet lidars and ozonesondes as well as their mean relative difference as function of  
241 altitude.

242 After the DISCOVER-AQ/FRAPPÉ campaign started, the TROPOZ lidar deployed to Fort Collins, CO to  
243 measure ozone. There were 11 ozonesonde profiles that were coincident and co-located with the TROPOZ  
244 measurements. The mean ozone profiles of TROPOZ and sondes (Figure 3a) show similar vertical variations with  
245 enhanced PBL and upper tropospheric ozone. The mean relative differences between TROPOZ and ozonesondes  
246 (Figure 3b) are mostly within  $\pm 10\%$  up to 9 km. The local maximum of the differences at 1.8 km is associated with  
247 the merging of ozone retrievals from the near-field channel and far-field channel. Above 9 km, the biases start to  
248 increase and exceed 25% with large oscillations due to large statistical errors as a consequence of low SNR. Biases  
249 between 10-20% are still very representative of the upper free troposphere. On average for altitudes from 0.35 to 12  
250 km, TROPOZ measures 2.9% higher ozone than the ozonesondes. This difference can be seen as the mean difference  
251 of ozone column average between the ozonesondes and lidar for a 30-min integration time.

252 Between July 10 and July 16, a total of 10 ozonesondes were released near the BAO tower and 7 of them  
253 were coincident with TOPAZ measurements (3 on July 10, 3 on July 11, and 1 on July 16). TOPAZ mostly agrees  
254 with ozonesondes between -5% and 10% (Figure 3 c, d). Compared to ozonesondes, TOPAZ generally measures  
255 more PBL ozone with an overall average of 4.4%.

256 On July 16, there was only one pair of coincident LMOL and ozonesonde measurements at the BAO tower  
257 (Figure 3 e, f). The 30-minute averaged LMOL ozone profile agrees with ozonesonde mostly within 0-15% between  
258 0.95 and 4.5 km AGL with an overall average of 6.2%. The maximum bias occurring at far range (above 4 km) is  
259 principally due to low SNR. The bias observed at 1.5 km is likely due to the high variation in aerosol concentration,  
260 that was also observed in the green channel. Since there is only one comparison between LMOL and ozonesonde, the  
261 statistical information on the overall bias between LMOL and the ozonesondes is not possible.



262 In summary, all three TOLNet lidars exhibit overall positive bias, up to 4.4%, compared to ozonesondes  
263 excluding the single profile comparison of LMOL (6.2%). The larger bias than the climatological difference  
264 between lidar and ozonesondes reported by Gaudel et al. (2015) (0.6 ppbv) could be associated with the much  
265 shorter averaging time period. The maximum biases exist in two regions, near-range altitudes and far-range  
266 altitudes. The large far-range bias is expected and is primarily associated with the high statistical errors arising from  
267 low SNR. The large near-range bias is more complicated and could be associated with various factors, primarily the  
268 aerosol correction and the merging of signal or ozone from different optical or altitude channels.

### 269 3.3 Lidars versus P-3B Chemiluminescence Instrument

270 During the campaigns, the P-3B aircraft measured ozone profiles while doing spirals above the lidar sites.  
271 There are 34 coincident profiles between TROPOZ and the P-3B at Fort Collins, 29 between TOPAZ and the P-3B at  
272 the BAO tower, and 9 between LMOL and the P-3B at Golden, CO. The distances between the lidar and P-3B spiral  
273 center for these paired profiles were less than 11 km. To make coincident pairs between P-3B and lidar data, we  
274 interpolate the P-3B data onto the lidar vertical grids with a 15-m vertical resolution. Figure 4 shows the average ozone  
275 profiles measured by the lidars and the P-3B as well as their mean relative differences. TROPOZ and the P-3B agree  
276 with each other within  $\pm 5\%$  between 0.5 to 3.5 km (Figure 4 a, b) with a -0.8% overall average relative difference.  
277 TOPAZ agrees with the P-3B within -11% and 3% between 0.5 and 2 km (Figure 4 c, d) with a -2.7% overall average  
278 relative difference. TOPAZ underestimates the lower-PBL (<1.5 km) ozone compared to P-3B, but when compared  
279 to ozonesondes TOPAZ overestimates ozone at many of these same altitudes (see Figure 3 d). LMOL agrees with P-  
280 3B mostly within -5-0% above 1800 m and within -15% and -5% between 0.7-1.8 km (Figure 4 e, f) with a -4.9%  
281 overall average relative difference.

282 In summary, TOPAZ and LMOL exhibited noticeable negative bias in the PBL compared to the P-3B while  
283 TROPOZ measured slightly lower than the P-3B. The differences between the two lidars and the P-3B are not  
284 significantly correlated suggesting that the problem was not likely from the P-3B ozone instrument. These differences  
285 could at least in part be caused by the lidar systematic errors we mentioned earlier in Section 2.1.5, but could also  
286 reflect horizontal ozone variability across the P-3B spirals, which were up to 22 km in diameter.

## 287 4. Summary and Conclusions

288 Intercomparisons have been made between three of the six TOLNet ozone lidars (NASA GSFC's TROPOZ,  
289 NOAA ESRL's TOPAZ, and NASA LaRC's LMOL) and between the lidars and other *in situ* ozone measurement  
290 instruments using coincident data during the 2014 DISCOVER-AQ and FRAPPÉ campaigns. On average, TROPOZ,  
291 TOPAZ, and LMOL reported very similar ozone within their reported uncertainties for a 5-min signal integration  
292 time. The three lidars measured consistent ozone variations revealed in the lidar time-height curtains and in the  
293 distribution of their relative differences. From intercomparisons between the lidars and other instruments we find (1)  
294 All lidars measure higher ozone than ozonesondes with an averaged relative difference within 4.4%. The lidar profile  
295 measurements agree with the ozonesonde observations within -10-15% in their measurable ranges except at a few  
296 near-field altitudes. These results are generally consistent with Sullivan et al. (2015) from a similar ozonesonde-lidar  
297 intercomparison. (2) TROPOZ agrees with the P-3B chemiluminescence Instrument below 3.5 km within  $\pm 5\%$  with a

298 small column-averaged relative difference of -0.8%. TOPAZ and LMOL exhibit a slightly larger bias mostly between  
299 -15% and 5% below 2 km compared to P-3B with a column-averaged difference of -2.7% and -4.9%, respectively.

300 Overall, the TOLNet lidars are capable of capturing high-temporal tropospheric ozone variability and  
301 measuring tropospheric ozone with accuracy better than  $\pm 15\%$  in terms of their vertical resolving capability and better  
302 than  $\pm 5\%$  in terms of their column measurement. These lidars have sufficient accuracy for model evaluation and  
303 satellite validation (Liu et al., 2010). Since the 2014 campaigns, improvements have been made on the TOLNET lidars  
304 to improve their stability and their accuracy. The validation of these modifications will be reported in a future paper.

### 305 **Acknowledgement**

306 This work is supported by the TOLNet program developed by the National Aeronautics and Space  
307 Administration (NASA)'s Science Mission Directorate and by the National Oceanic and Atmospheric Administration  
308 Earth System Research Laboratory. The views, opinions, and findings contained in this report are those of the authors  
309 and should not be construed as an official NOAA, NASA, or U.S. Government position, policy, or decision.

310

Table 1. Specifications for the TOLNet lidars.

	<b>TROPOZ</b>	<b>TOPAZ</b>	<b>LMOL</b>
<b>Transmitter</b>			
Laser type	Nd:YAG pumped D <sub>2</sub> , H <sub>2</sub> Raman cell	Nd:YLF pumped Ce:LiCAF	Nd:YLF pumped Ce:LiCAF
Wavelengths (nm)	288.9, 299.1	287, 291, 294	287.1, 292.7
Pulse Repetition Rate (Hz)	50	333	500
Pulse energy (mJ)	12 (299 nm), 16 (289 nm)	~0.06 for all wavelengths	0.2 for both wavelengths
<b>Detection and data acquisition system</b>			
Telescope diameter (cm)	45, 2.5	50	40, 30
FOV (mrad)	1 (45 cm), 10 (2.5 cm)	1.5 (far field channel), 3 (near field channel)	1.4 (far field channel), variable FOV (near field channel)
Signal detection type	PMT	PMT	PMT
Data acquisition type	PC	Analog	Analog and PC
Fundamental range resolution (m)	15	6	7.5
Instrument reference	(Sullivan et al., 2014)	(Alvarez et al., 2011)	(DeYoung et al., 2017)
<b>DIAL retrieval</b>			
DIAL retrieval and smoothing method	1 <sup>st</sup> -order (differential) SG filter with a 2 <sup>nd</sup> degree polynomial with an increasing window width applied on the derivative of the logarithm of the signal ratios	five-point least square fitting with a 450-m window applied on the derivative of the logarithm of the signal ratios	1 <sup>st</sup> -order (differential) SG filter with a 2 <sup>nd</sup> degree polynomial, with an increasing window width applied on the derivative of the logarithm of the signal ratios
Retrieval effective resolution (m)	~100 at 1 km degrading to ~800 at 10 km	~10 below 50 m, ~30 from 50 to 150 m, ~100 from 150 to 500 m, 315 above 500 m	225 below 3 km degrading to 506 above 3 km
Aerosol correction reference	(Kuang et al., 2011; Sullivan et al., 2014)	(Alvarez et al., 2011)	(Browell et al., 1985; DeYoung et al., 2017)
Valid altitudes (km above ground level, AGL)	0.35-16	0.01-2	0.7-4.5
<b>Measurement location</b>			
Latitude (°N)	40.050	40.045	40.050
Longitude (°W)	105.000	105.006	105.004
Elevation (m ASL)	1584	1587	1584

314 **Table 2. Estimated uncertainties for TROPOZ, TOPAZ and LMOL ozone measurements within their measurable range**  
 315 **(see Table 1) for the 5 or 30-min integration time.**

Source	Uncertainty	
	5-min integration	30-min integration
Statistical error	<20%	<8%
Aerosol interference	<10%	
Interference by SO <sub>2</sub> , NO <sub>2</sub> , O <sub>2</sub> dimmer	<1.5%	
Differential Rayleigh scattering	<1%	
Total*	<22%	13%

316 \*Total root-mean-square error.

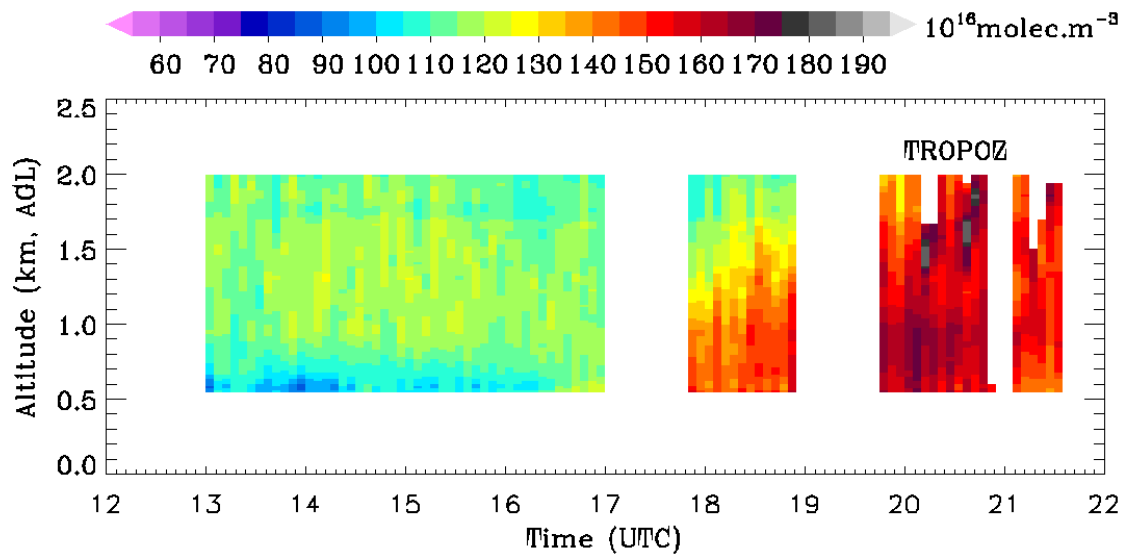
317  
 318  
 319  
 320  
 321  
 322  
 323  
 324  
 325  
 326  
 327  
 328

**Table 3. Comparisons of the ozone column average measured by TROPOZ, TOPAZ, and LMOL.**

Date	UTC time range	Lidar	Number of the paired profiles	Mean ozone column average (10 <sup>16</sup> molec·m <sup>-3</sup> )	1σ of the ozone column average (10 <sup>16</sup> molec·m <sup>-3</sup> )	Mean relative difference *	1σ of the difference
7/11/2014	1300 - 2135	TROPOZ/TOPAZ	80	127.3/128.6	17.8/16.7	-1.1%	2.6%
7/16/2014	1335 - 1730	LMOL/TOPAZ	28	98.1/102.0	13.1/13.0	-3.8%	2.9%

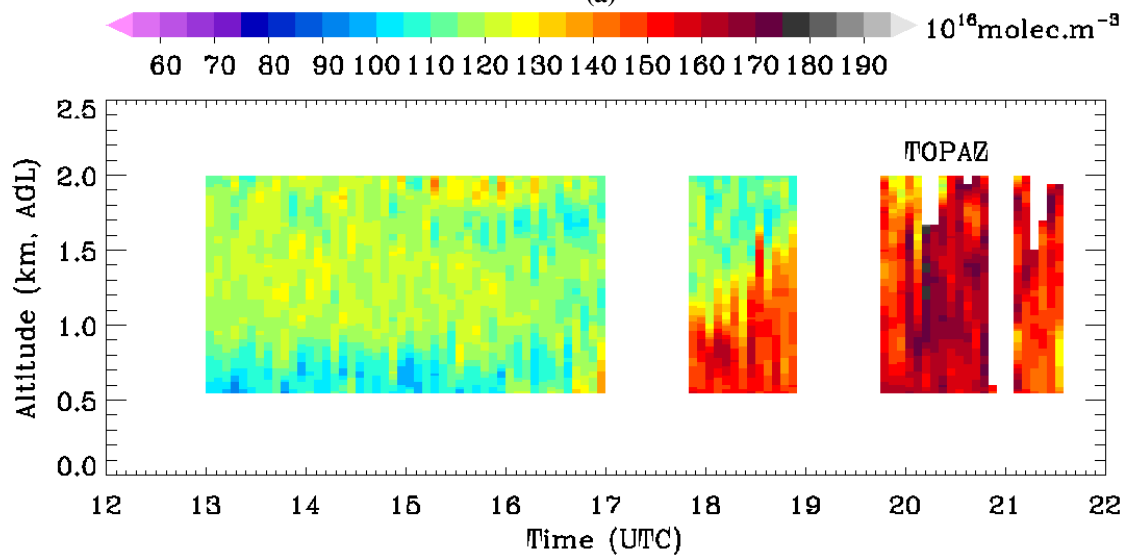
329 \* Equal to mean (A-B)/B for A/B in 'Lidar' column for all paired profiles.

330



331  
332

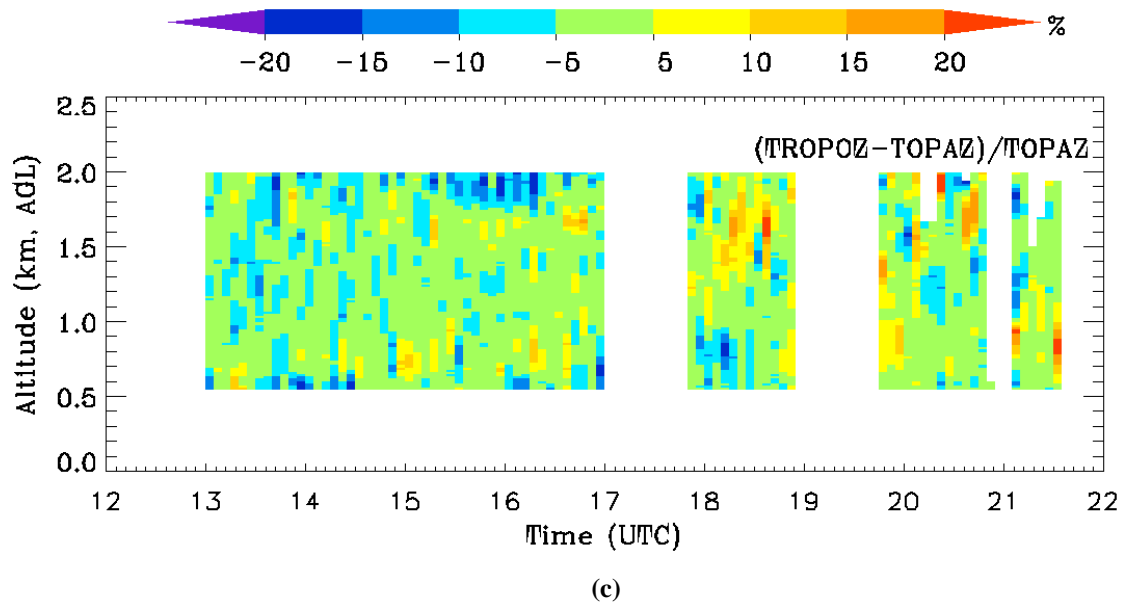
(a)



333  
334

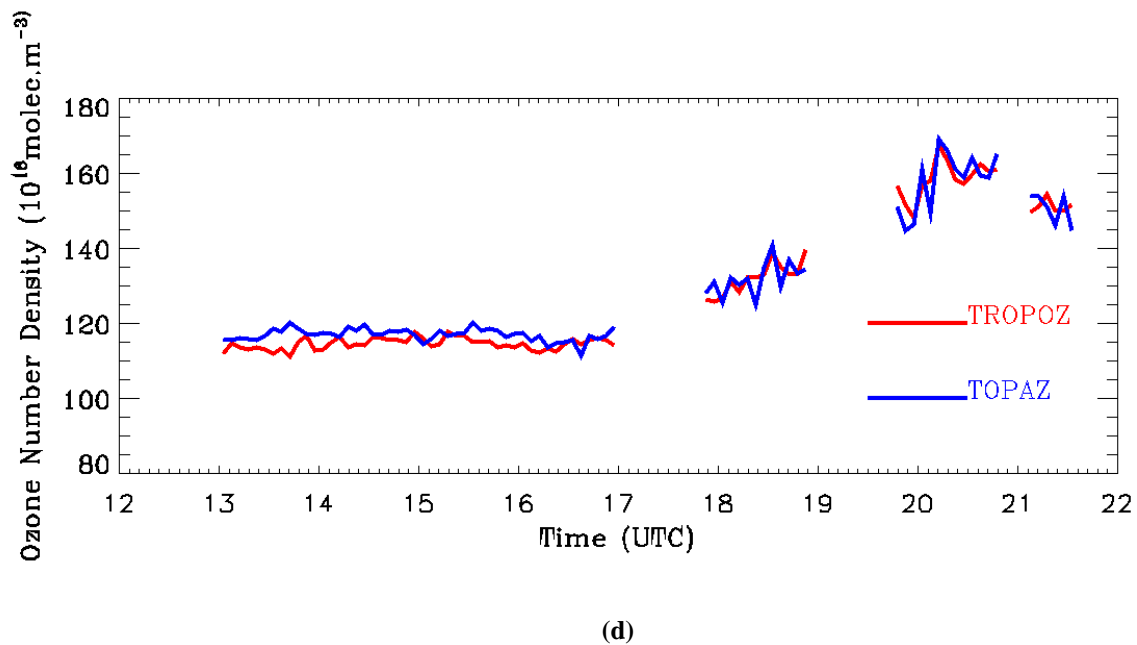
(b)

335



336

337



338

339

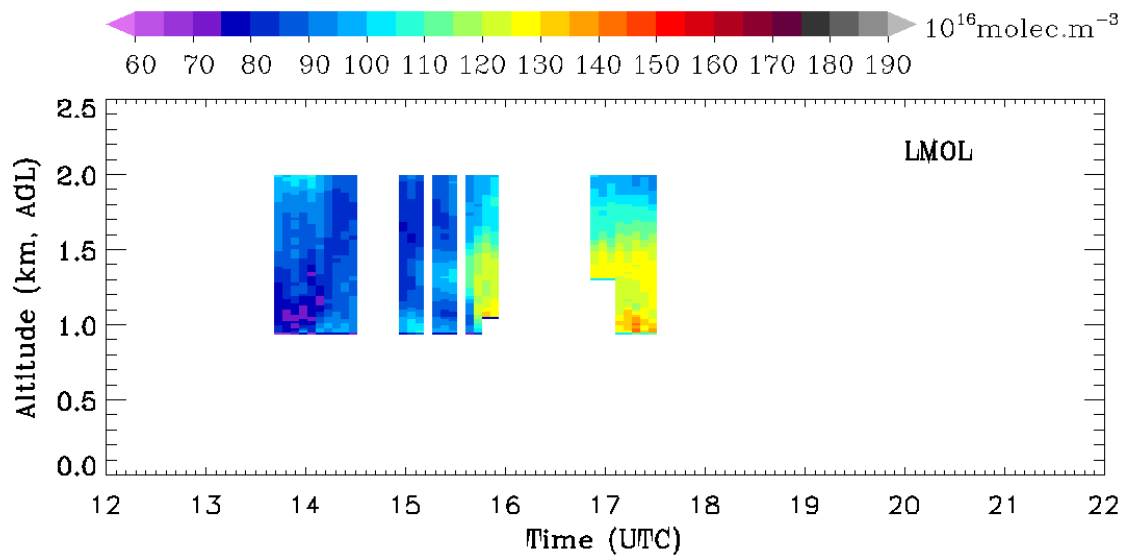
340 Figure 1. Comparisons of ozone measured by TROPOZ and TOPAZ. (a) Ozone number densities measured by TROPOZ.

341 (b) Ozone number densities measured by TOPAZ. (c) Their relative percent differences,  $(\text{TROPOZ} - \text{TOPAZ}) / \text{TOPAZ}$ . (d)

342 Column averages measured by the TROPOZ and TOPAZ. TROPOZ measures  $1.1 \pm 2.6\%$  lower ozone column average than

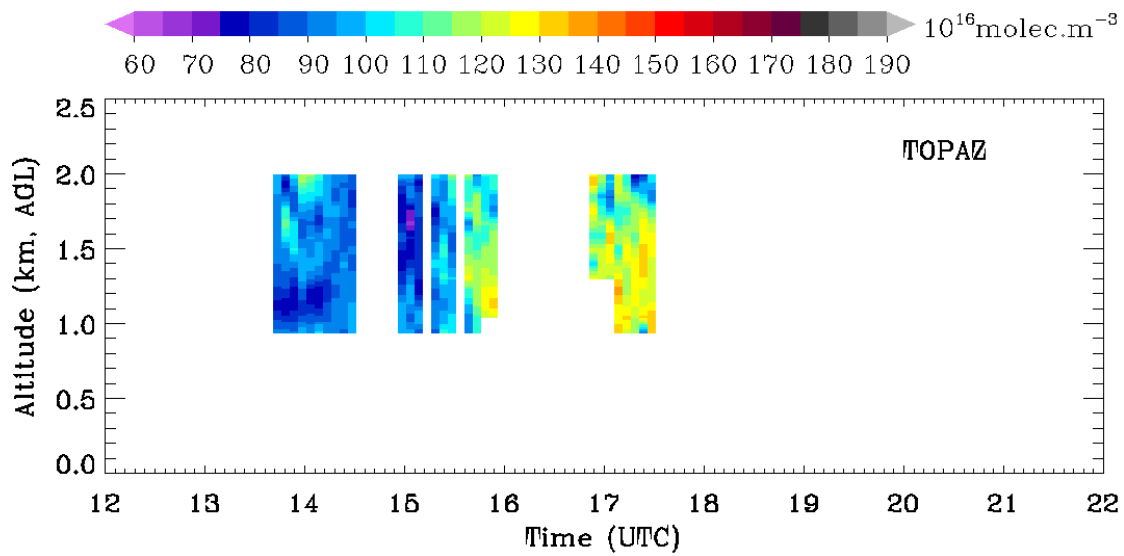
343 TOPAZ.

344



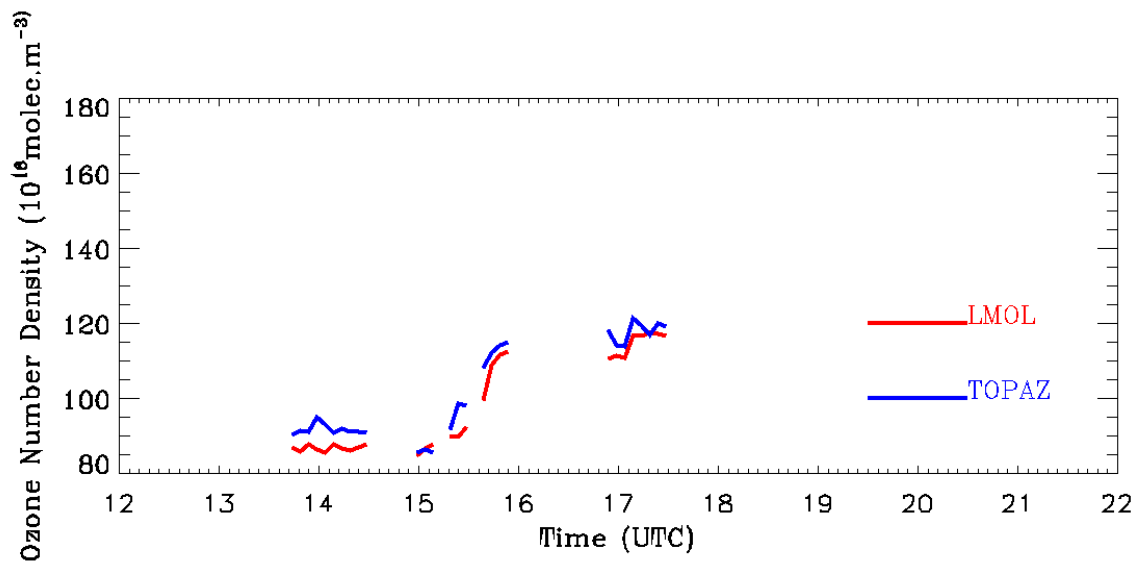
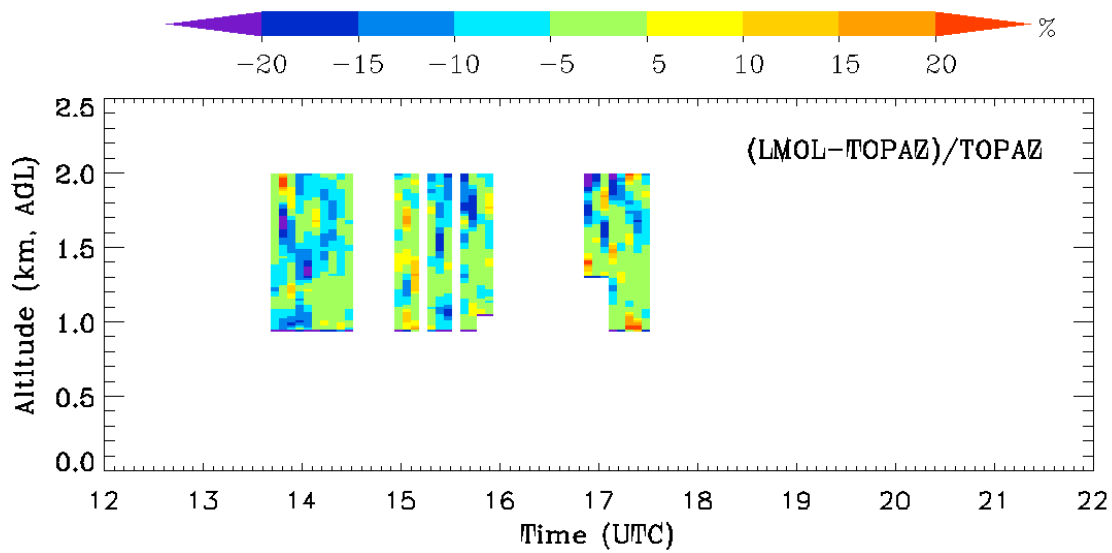
345  
346

(a)



347  
348

(b)



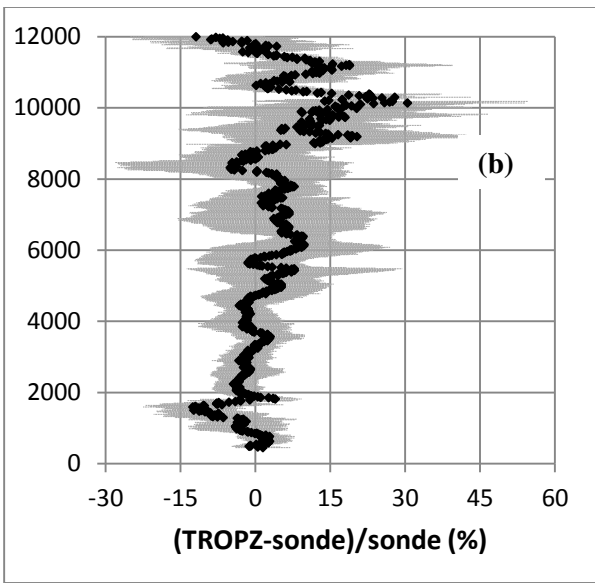
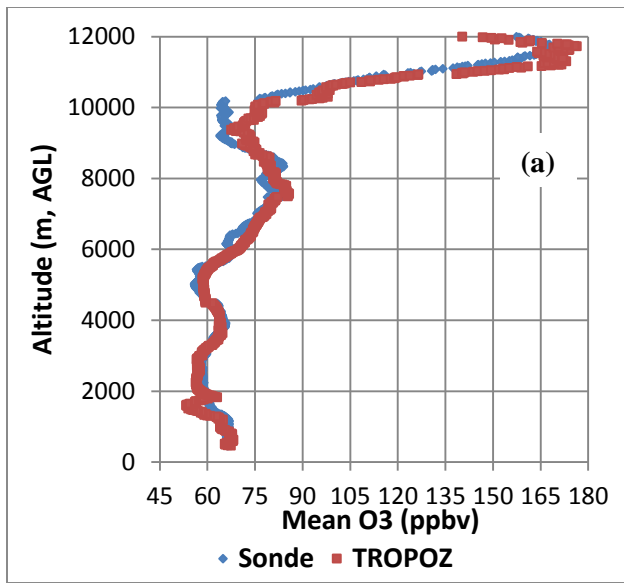
349  
350

351  
352  
353  
354  
355  
356

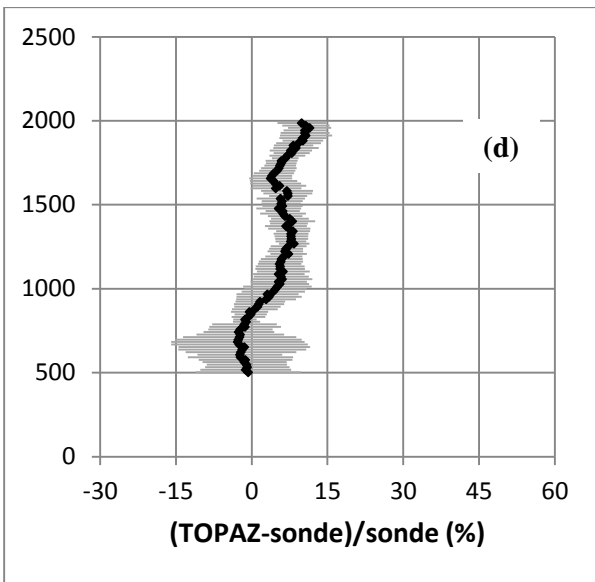
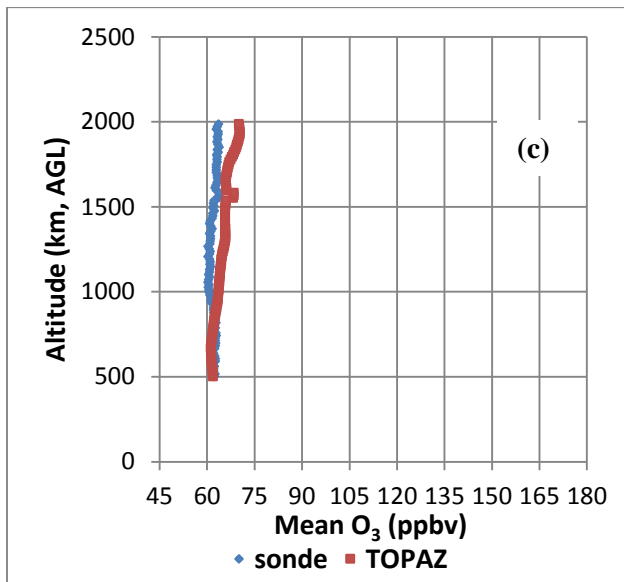
Figure 2. Comparisons of ozone measured by LMOL and TOPAZ. (a) LMOL-measured ozone number densities. (b) TOPAZ-measured ozone number densities. (c) Their relative percent differences,  $(LMOL - TOPAZ) / TOPAZ$ . (d) Column averages measured by LMOL and TOPAZ. LMOL measures  $3.8 \pm 2.9\%$  lower ozone column average than TOPAZ.

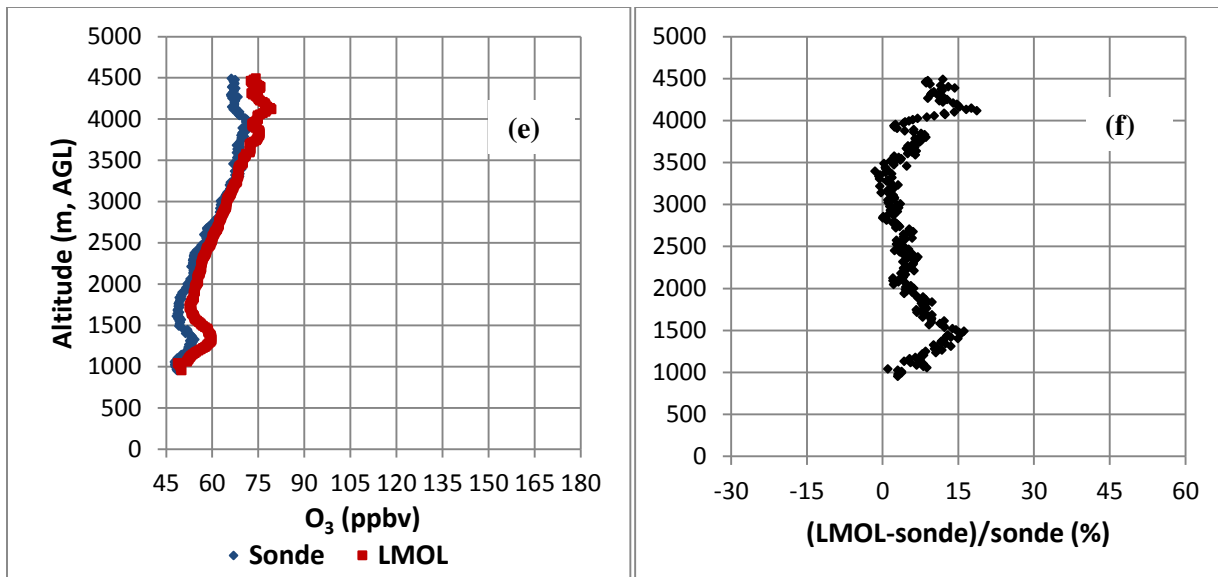


357



358





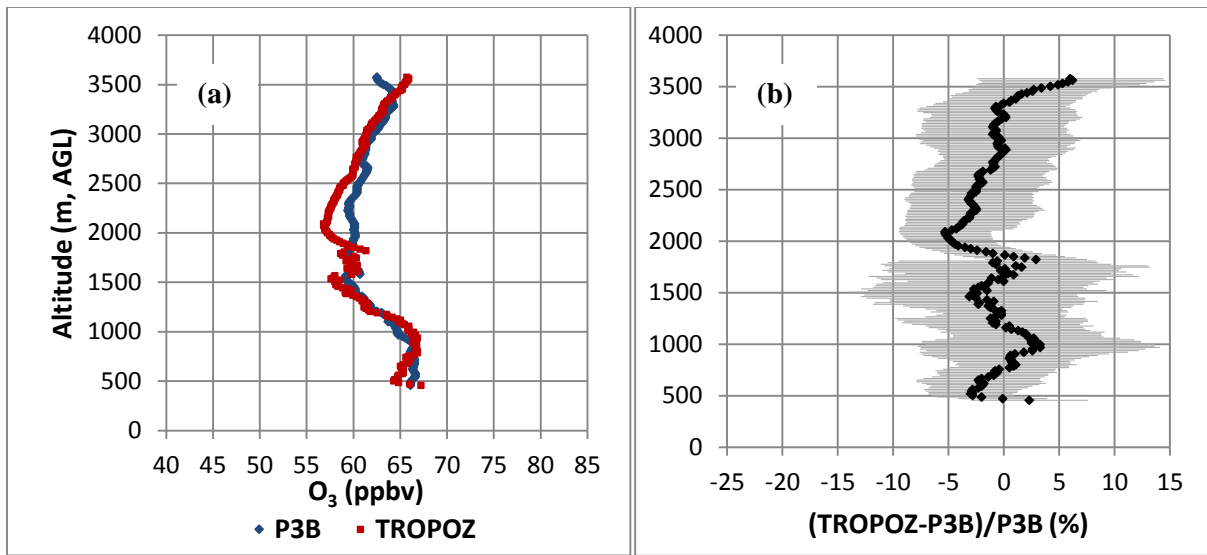
359

360 Figure 3. Comparisons of lidar and ozonesonde measurements. (a) Average ozone profiles measured by TROPOZ and  
 361 ozonesondes at Fort Collins, CO (11 pairs). (b) Mean relative difference between TROPOZ and ozonesondes as well as the  
 362 1- $\sigma$  standard deviations. (c) Average ozone profiles measured by TOPAZ and ozonesondes at BAO Tower (7 pairs). (d)  
 363 Mean relative difference between TOPAZ and ozonesondes. (e) Average ozone profiles measured by LMOL and ozonesonde  
 364 at the BAO tower (1 pair). (f) Relative difference between LMOL and ozonesonde.

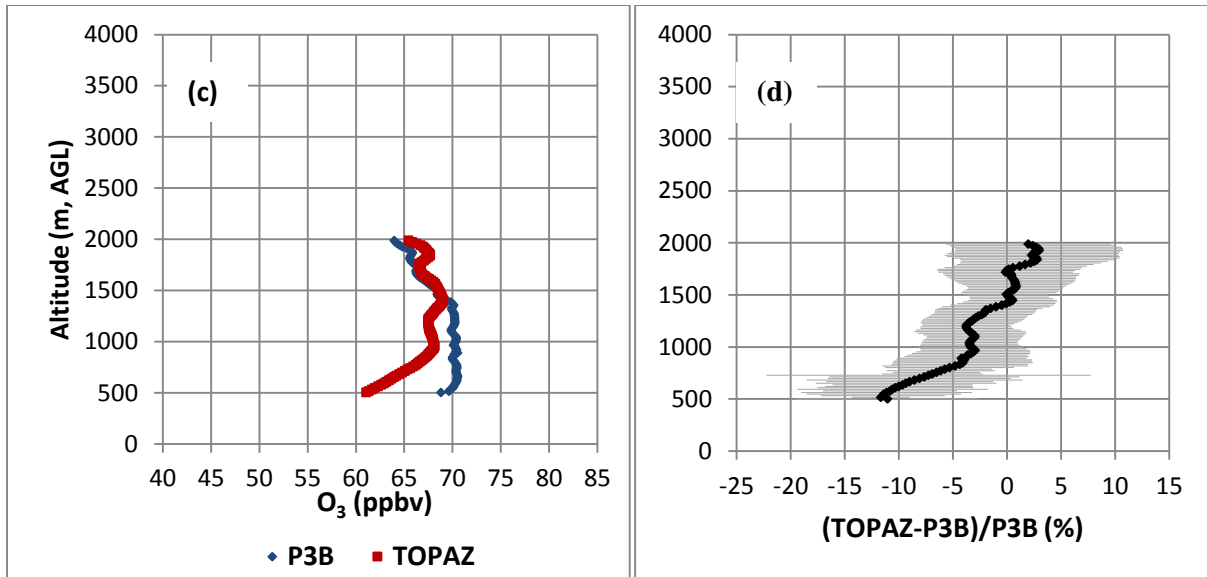
365

366

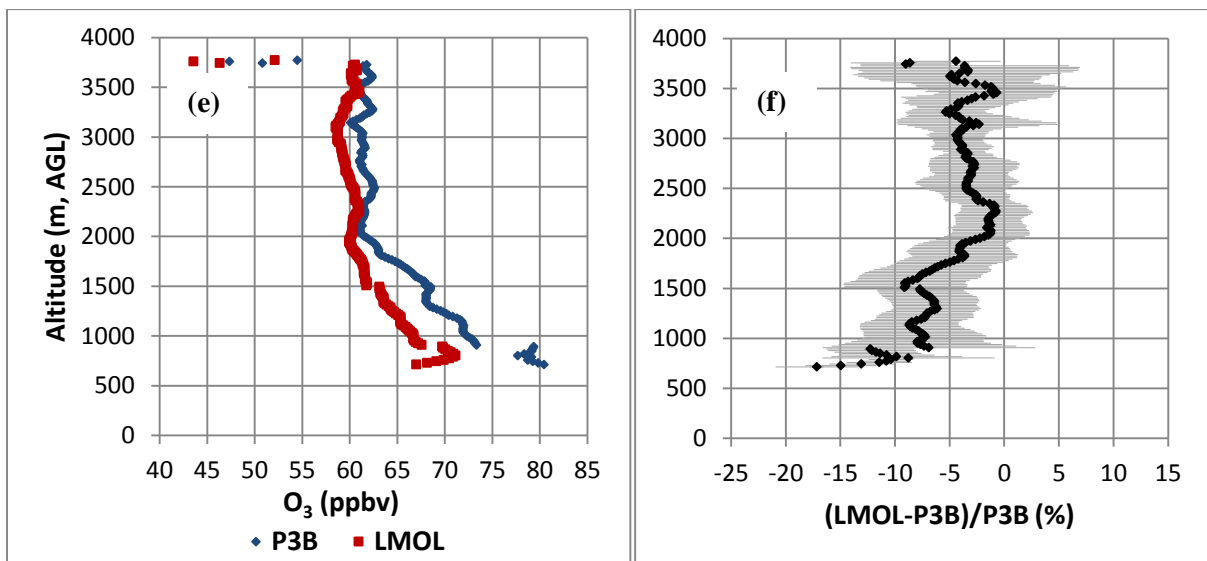
367



368



369



370

(e)

(f)

371 **Figure 4. Intercomparison between the lidar and P-3B measurements. (a) Average ozone profiles measured by TROPOZ**  
 372 **and P3B at Fort Collins, CO (34 profiles). (b) Mean relative difference between TROPOZ and P-3B data as well as the 1- $\sigma$**   
 373 **standard deviation. (c) Average ozone profiles measured by TOPAZ and P-3B at the BAO Tower (29 profiles). (d) Mean**  
 374 **relative difference between TOPAZ and P-3B data. (e) Average ozone profiles measured by LMOL and P-3B at Golden,**  
 375 **CO (9 profiles). (f) Mean relative difference between LMOL and P-3B data.**

376

377

## References

378

- 379 Alvarez, R. J., Senff, C. J., Langford, A. O., Weickmann, A. M., Law, D. C., Machol, J. L., Merritt, D. A., Marchbanks,  
 380 R. D., Sandberg, S. P., Brewer, W. A., Hardesty, R. M., and Banta, R. M.: Development and Application of  
 381 a Compact, Tunable, Solid-State Airborne Ozone Lidar System for Boundary Layer Profiling, *J. Atmos.*  
 382 *Oceanic Tech.*, 28, 1258-1272, 10.1175/JTECH-D-10-05044.1, 2011.
- 383 Bowman, K. W.: Toward the next generation of air quality monitoring: Ozone. *Atmos. Environ.*, 80, 571-583, 2013.
- 384 Brion, J., Chakir, A., Daumont, D., and Malicet, J.: High-resolution laboratory absorption cross section of O<sub>3</sub>  
 385 temperature effect, *Chem. Phys. Lett.*, 213, 510-512, 1993.
- 386 Browell, E. V., Ismail, S., and Shipley, S. T.: Ultraviolet DIAL measurements of O<sub>3</sub> profiles in regions of spatially  
 387 inhomogeneous aerosols, *Appl. Opt.*, 24, 2827-2836, 1985.
- 388 Crawford, J. H., and Pickering, K. E.: DISCOVER-AQ: Advancing strategies for air quality observations in the next  
 389 decade, *Environ. Manage.*, 4-7, 2014.
- 390 Daumont, D., Brion, J., Charbonnier, J., and Malicet, J.: Ozone UV spectroscopy I: Absorption cross-sections at room  
 391 temperature, *J. Atmos. Chem.*, 15, 145-155, 1992.
- 392 De Young, R., Carrion, W., Ganoe, R., Pliutau, D., Gronoff, G., Berkoff, T., and Kuang, S.: Langley mobile ozone  
 393 lidar: ozone and aerosol atmospheric profiling for air quality research, *Appl. Opt.*, 56, 721,  
 394 10.1364/ao.56.000721, 2017.
- 395 Deshler, T., Mercer, J. L., Smit, H. G. J., Stubi, R., Levrat, G., Johnson, B. J., Oltmans, S. J., Kivi, R., Thompson, A.  
 396 M., Witte, J., Davies, J., Schmidlin, F. J., Brothers, G., and Sasaki, T.: Atmospheric comparison of  
 397 electrochemical cell ozonesondes from different manufacturers, and with different cathode solution strengths:  
 398 The balloon experiment on standards for ozonesondes., *J. Geophys. Res.*, 113, D04307, doi:  
 399 10.1029/2007/JD008975, 2008.
- 400 Dingle, J. H., Vu, K., Bahreini, R., Apel, E. C., Campos, T. L., Flocke, F., Fried, A., Herndon, S., Hills, A. J.,  
 401 Hornbrook, R. S., Huey, G., Kaser, L., Montzka, D. D., Nowak, J. B., Reeves, M., Richter, D., Roscioli, J.  
 402 R., Shertz, S., Stell, M., Tanner, D., Tyndall, G., Walega, J., Weibring, P., and Weinheimer, A.: Aerosol  
 403 optical extinction during the Front Range Air Pollution and Photochemistry Experiment (FRAPPÉ) 2014  
 404 summertime field campaign, Colorado, USA, *Atmos. Chem. Phys.*, 16, 207-217, doi:10.5194/acp-16-11207-  
 405 2016, 2016.
- 406 Eisele, H., and Trickl, T.: Improvements of aerosol algorithm in ozone lidar data processing by use of evolutionary  
 407 strategies, *Appl. Opt.*, 44, 2638-2651, 2005.
- 408 Gaudel, A., Ancellet, G. and Godin-Beekmann, S.: Analysis of 20 years of tropospheric ozone vertical profiles by  
 409 lidar and ECC at Observatoire de Haute Provence (OHP) at 44 N, 6.7 E, *Atmos. Environ.*, 113, 78-89, 2015.
- 410 Godin, S. M., Carswell, A. I., Donovan, D. P., Claude, H., Steinbrecht, W., McDermid, I. S., McGee, T. J., Gross, M.  
 411 R., Nakane, H., Swart, D. P. J., Bergwerff, H. B., Uchino, O., Gathen, P. v. d., and Neuber, R.: Ozone  
 412 differential absorption lidar algorithm intercomparison, *Appl. Opt.*, 38, 6225-6236, 1999.
- 413 Immler, F.: A new algorithm for simultaneous ozone and aerosol retrieval from tropospheric DIAL measurements,  
 414 *Appl. Phys. B*, 76, 593-596, 2003.
- 415 Johnson, B. J., Helmig, D., and Oltmans, S.: Evaluation of ozone measurements from a tethered balloon-sampling  
 416 platform at South Pole Station in December 2003, *Atmos. Environ.*, 42, 2780-2878,  
 417 10.1016/j.atmosenv.2007.03.043, 2008.
- 418 Komhyr, W. D.: Electrochemical cells for gas analysis, *Ann. Geophys.*, 25, 203-210, 1969.
- 419 Komhyr, W. D., Barnes, R. A., Brothers, G. B., Lanthrop, J. A., and Opperman, D. P.: Electrochemical concentration  
 420 cell ozonesonde performance evaluation during STOIC 1989, *J. Geophys. Res.*, 100, 9231-9244, 1995.

421 Kovalev, V. A., and Bristow, M. P.: Compensational three-wavelength differential-absorption lidar technique for  
422 reducing the influence of differential scattering on ozone-concentration measurements, *Appl. Opt.*, 35, 4790-  
423 4797, 1996.

424 Kuang, S., Burris, J. F., Newchurch, M. J., Johnson, S., and Long, S.: Differential Absorption Lidar to Measure  
425 Subhourly Variation of Tropospheric Ozone Profiles, *IEEE Transactions on Geoscience and Remote Sensing*,  
426 49, 557-571, 10.1109/TGRS.2010.2054834, 2011.

427 Kuang, S., Newchurch, M. J., Burris, J., and Liu, X.: Ground-based lidar for atmospheric boundary layer ozone  
428 measurements, *Appl. Opt.*, 52, 3557-3566, 10.1364/AO.52.003557, 2013.

429 Langford, A. O., Senff, C. J., Alvarez II, R. J., Banta, R. M., Hardesty, M., Parrish, D. D., and Ryerson, T. B.:  
430 Comparison between the TOPAZ airborne ozone lidar and in situ measurements during TexAQS 2006, *J.*  
431 *Atmos. Oceanic Technol.*, 28, 1243-1257, doi: <http://dx.doi.org/10.1175/JTECH-D-10-05043.1> 2011.

432 Langford, A. O., Alvarez, R. J., Brioude, J., Fine, R., Gustin, M., Lin, M. Y., Marchbanks, R. D., Pierce, R. B.,  
433 Sandberg, S. P., Senff, C. J., Weickmann, A. M., and Williams, E. J.: Entrainment of stratospheric air and  
434 Asian pollution by the convective boundary layer in the Southwestern U.S, *Journal of Geophysical Research:*  
435 *Atmospheres*, n/a-n/a, 10.1002/2016JD025987, 2016.

436 Leblanc, T., Sica, R. J., van Gijsel, J. A. E., Godin-Beekmann, S., Haefele, A., Trickl, T., Payen, G., and Gabarrot, F.:  
437 Proposed standardized definitions for vertical resolution and uncertainty in the NDACC lidar ozone and  
438 temperature algorithms – Part 1: Vertical resolution, *Atmos. Meas. Tech.*, 9, 4029-4049, 10.5194/amt-9-  
439 4029-2016, 2016.

440 Liu, X., Bhartia, P. K., Chance, K., Spurr, R. J. D., and Kurosu, T. P.: Ozone profile retrievals from the Ozone  
441 Monitoring Instrument, *Atmos. Chem. Phys.*, 10, 2521-2537, 2010.

442 Malicet, C., Daumont, D., Charbonnier, J., Parisse, C., Chakir, A., and Brion, J.: Ozone UV spectroscopy. II.  
443 Absorption cross-sections and temperature dependence, *J. Atmos. Chem.*, 21, 263-273, 1995.

444 McDermid, I. S., Godin, S. M., Lindqvist, L. O., Walsh, T. D., Burris, J., Butler, J., Ferrare, R., Whiteman, D., and  
445 McGee, T. J.: Measurement intercomparison of the JPL and GSFC stratospheric ozone lidar systems, *Appl.*  
446 *Opt.*, 29, 4671-4676, 1990.

447 Newchurch, M. J., Kuang, S., Leblanc, T., Alvarez, R. J., Langford, A. O., Senff, C. J., Burris, J. F., McGee, T. J.,  
448 Sullivan, J. T., DeYoung, R. J., and Al-Saadi, J.: TOLNET - A Tropospheric Ozone Lidar Profiling Network  
449 for Satellite Continuity and Process Studies, *The 27th International Laser Radar Conference (ILRC 27)*, 2016,

450 Papayannis, A., Ancellet, G., Pelon, J., and Mégie, G.: Multiwavelength lidar for ozone measurements in the  
451 troposphere and the lower stratosphere, *Appl. Opt.*, 29, 467-476, 1990.

452 Ridley, B. A., Grahek, F. E., and Walega, J. G.: A small high-sensitivity, medium-response ozone detector suitable  
453 for measurements from light aircraft, *J. Atmos. Oceanic Tech.*, 9, 142-148, 1992.

454 Senff, C. J., Alvarez, R. J., Hardesty, R. M., Banta, R. M., and Langford, A. O.: Airborne lidar measurements of ozone  
455 flux downwind of Houston and Dallas, *J. Geophys. Res.: Atmospheres*, 115, n/a-n/a,  
456 10.1029/2009JD013689, 2010.

457 Smit, H. G. J., Straeter, W., Johnson, B. J., Oltmans, S. J., Davies, J., Tarasick, D. W., Hoegger, B., Stubi, R.,  
458 Schmidlin, F. J., Northam, T., Thompson, A. M., Witte, J. C., Boyd, I., and Posny, F.: Assessment of the  
459 performance of ECC-ozonesondes under quasi-flight conditions in the environmental simulation chamber:  
460 Insights from the Juelich Ozone Sonde Intercomparison Experiment (JOSIE), *J. Geophys. Res.*, 112, D19306,  
461 doi:10.1029/2006JD007308, 2007.

462 Stauffer, R. M., Morris, G. A., Thompson, A. M., Joseph, E., Coetzee, G. J. and Nalli, N. R.: Propagation of radiosonde  
463 pressure sensor errors to ozonesonde measurements, *Atmos. Meas. Tech.*, 7, 65-79, 2014.

464 Steinbrecht, W., McGee, T. J., Twigg, L. W., Claude, H., Schönerborn, F., Sumnicht, G. K., and Silbert, D.:  
465 Intercomparison of stratospheric ozone and temperature profiles during the October 2005 Hohenpeißenberg  
466 Ozone Profiling Experiment (HOPE), *Atmos. Meas. Tech.*, 2, 125-145, 2009.

467 Sullivan, J. T., McGee, T. J., Sumnicht, G. K., Twigg, L. W., and Hoff, R. M.: A mobile differential absorption lidar  
468 to measure sub-hourly fluctuation of tropospheric ozone profiles in the Baltimore-Washington, D.C. region,  
469 *Atmos. Meas. Tech.*, 7, 3529-3548, 10.5194/amt-7-3529-2014, 2014.

470 Sullivan, J. T., McGee, T. J., DeYoung, R., Twigg, L. W., Sumnicht, G. K., Pliutau, D., Knepp, T., and Carrion, W.:  
471 Results from the NASA GSFC and LaRC Ozone Lidar Intercomparison: New Mobile Tools for Atmospheric  
472 Research, *J. Atmos. Oceanic Tech.*, 32, 1779-1795, doi:10.1175/JTECH-D-14-00193.1, 2015.

473 Weinheimer, A. J., Walega, J. G., Ridley, B. A., Satche, G. W., Anderson, B. E., and Collins Jr., J. E.: Stratospheric  
474 NO<sub>y</sub> measurements on the NASA DC-8 during AASE II, *Geophys. Res. Lett.*, 20, 2563-2566, 1993.

475